Optical Characterization of a 1-D Nanostructure by Dark-Field Microscopy and Surface Plasmon Resonance to Determine Biomolecular Interactions

Hui-Hsin Lu, Tzu-Chien Hsiao, Su-Ming Hsu, and Chii-Wann Lin, *Member, IEEE*

***Abstract*—This paper presents a multifunctional imaging system that combines dark-field microscopy (DFM) with spectroscopy to image nanostructures and identify their optical properties from absorption spectra. The optical resolving power of this system is determined using a 1-D nanostructure with pitches of 120, 390, and 770 nm with four formats of optical disks. These pattern sizes are verified by atomic force microscopy (AFM) first. The results demonstrate that the resolving power of current system setup can down to 86 nm. The resultant DFM images appear to be slightly larger than the AFM images. A 50-nm-thick gold film was then deposited on top of these nanostructures, and their absorption spectra were obtained to elucidate its optical properties, enhanced by surface plasmon resonance. The immobilization of streptavidin on the surface of gold-coated nanostructure causes the absorption spectra to shift from 600 to 610 nm. A protein nanoarray with a dot size of 50 nm was also imaged by DFM, and can be implemented as a potential biochemical diagnostic system on an optical disk format. Specimens of adenocarcinoma cells and ovary cancer cells were also imaged using this DFM system, and the nuclei structure and some cellular organs can be recognized using a 100× objective oil lens.**

***Index Terms*—1-D nanostructure, surface plasmon, dark-field microscopy (DFM).**

I. Introduction

THE low-dimensional nanostructure made by metal and semiconductor materials exhibits a strong optical enhancement effect as electron transitions due to quantum confinement. Measuring the optical properties of these nanostructures can help to confirm some of their physical characteristics. Various optical approaches, such as obtaining the absorption spectrum, emission spectrum, vibration spectrum, scattering spectrum, and the intensity of polarization, have been applied to elucidate these characteristics. For instance, the absorption spectrum of gold or silver nanoparticles represents the resonance bands of its surface electrons, produced by light field coupling. Surface enhanced Raman scattering (SERS) spectrum is employed to observe the Raman shift of the molecular vibration bands caused by the interaction with the surface plasmon of noble metal nanostructures [1]–[3]. Advanced nonlinear optical approaches, such as two-photon absorption, have also been used to obtain information on the interband transition associated with quantum wells or quantum dots [4], [5]. Accordingly, advanced optical techniques must be continually improved to obtain more detailed information on physical phenomena and characterize nanostructures, which are revealed by the measured optical signals.

A combination of the spectral scheme and optical microscopy has become extensively utilized in research on biophotonics because of the combined capabilities to fingerprint the microenvironment and near-surface interactions. Many nanostructures with unique optical characteristics have been employed to enhance the measurement of molecular interaction from biological specimens. For example, quantum dots have replaced traditional molecular probes for labeling biomolecules because of their better stability and efficiency of luminance. Moreover, noble metal nanoparticles have been used to enhance the intensity of fluorescence, thus improving the sensitivity of detection of the biomolecular interaction, because some of these biomolecules are present in extremely low concentrations in the cell and tissue [6]–[10]. However, to study biological phenomena on the nanometer scale or even on the scale of single molecules, the limits of optical resolution must be overcome. Recent investigations have discovered that some noble metal nanostructures with negative permittivity that were exposed by the scanning near-field microscopy (SNOM) can be imaged to improved the resolution (from a half wavelength to one seventh of a wavelength) based on the focusing of evanescent waves [11], [12]. Stimulated emission depletion (STED) microscopy is another approach for improving the resolution beyond the diffraction limit; this is accomplished by sharpening the focus of the fluorescent spot, depending on a short excitation pulse coupled with a long depletion pulse in a microscope objective [13], [14]. Researchers have utilized a range of microscopes with dark-field microscopy (DFM) to observe the optical properties of individual gold and silver nanoparticles and nanorods because DFM can block the background interference, and improve overall image quality and contrast [15], [16].

Manuscript received November 02, 2008; revised February 24, 2009; accepted May 24, 2009. Current version published February 24, 2010. This work was supported in part by the National Science Council of the Republic of China, Taiwan, under Contract NSC 95-2218-E-002-054-MY3 and Contract NSC 94-3114-P-002-002-Y. The associate editor coordinating the review of this paper and approving it for publication was Dr. Dwight Woolard.

H.-H. Lu is with the Institute of Biomedical Engineering, National Taiwan University, Taipei 106, Taiwan (e-mail:d94921033@ntu.edu.tw).

T.-C. Hsiao is with the Institute of Biomedical Engineering and the Department of Computer Science, National Chiao-Tung University, Hsinchu 300, Taiwan(e-mail: labview@cs.nctu.edu.tw).

S.-M. Hsu is with the Department of Pathology, College of Medicine, National Taiwan University, Taipei 100, Taiwan (e-mail: suminghsu@ntu.edu.tw).

C.-W. Lin is with the Institute of Biomedical Engineering, Institute of Bioelectronics and Bioinformatics, and the Institute of Applied Mechanics, National Taiwan University, Taipei 106, Taiwan (e-mail: cwlinx@ntu.edu.tw).

Color versions of one or more of the figures in this paper are available online at http://ieeexplore.ieee.org.

Digital Object Identifier 10.1109/JSEN.2009.2038628

This paper presents a multifunctional DFM system with a spectrographic system to measure 1-D nanostructures on commercially available storage disks. Various sizes of 1-D nanostructures were imaged using white light and 390 nm UV laser light to determine the resolving ability of the DFM system. The absorption spectra of these 1-D structures coated with thin gold layers were then obtained and considered in the light of the plasmonic absorption properties. Then, a protein nanoarray with a diameter of 50 nm was also imaged by DFM to evaluate the possibility of implementing a practical optical diagnostic system using the optical disk layout. Finally, cellular structures were observed by DFM with and without staining to determine the potential of using noble metal nanostructures to image the intracellular structure in the future.

II. Materials and Methods

A. Preparation of One-Dimensional Nanostructure

One-dimensional nanostructures with various widths were obtained from the track patterns of commercial optical storage disks - a 25G Blu-ray Disc, an 8.5G DVD, a 4.7G DVD, and a VCD. A whole disk was cut into two semicircles using a general craft knife to separate the layers of the optical disk from each other. The disk protection layer was torn with sharp tweezers and then cut into small pieces of 0.5 cm by 0.5 cm before it was imaged by DFM and AFM. The track size of each optical disk was determined by atomic force microscopy to provide a reference for DFM imaging. To identify the optical properties of one-dimensional nanostructures, a thin gold layer of 50 nm thickness was deposited on the surface of the exposed optical disks using electron beam evaporation (ULVAC Company, Japan).

B. Deposition of Biomolecules and Cellular Samples

All chemicals used in this work were purchased from Sigma Chemical Company. Mercaptododecanoic acid at a concentration of 5 mM was dissolved in deionized water before use. A droplet of this solution was put on the gold surface of the disk for 15 minutes to act as a linker between the gold surface and biomolecules. A carboxylic group (COOH) bond was activated by 1-ethyl-3- (3-dimethylaminopropyl) carbodiimide (EDC) (0.1 M in water). NHS-biotin (10 mM, Pierce, IL, U.S.A.) and streptavidin (0.14 mM, Invitrogen, Cal., U.S.A.) were diluted by adding 1X phosphate buffered saline (PBS) buffer solution. After it had been immobilized with biotin and then washed by PBS, streptavidin was added and left to hybridize for 20 minutes. Finally, water was employed to remove the residual reagent before the chip was dried in nitrogen gas in preparation for AFM scanning.

In forming a nanoarray on silicon surface, an n-type silicon surface that was treated with hydrofluoric solution to remove the native oxide layer, and then atomic force microscopy with bias control (NanoInk, IL, U.S.A.) was applied to fabricate silicon dioxide nanodots with a diameter of 50 nm on the silicon surface. The applied bias was 30 V and the patterning speed was 0.1 s per dot. According to the referenced method [17], mercaptopropyltrimethoxysilan (MPTMS) (1% in ethanol) and a hetero-bifunctional crosslinker, N-gamma- maleimidobutyryloxy succinimide ester (GMBS) (0.25 mM in ethanol), were used to form an amine-modified surface of silicon dioxide on a prepared nano-biochip. MPTMS and GMBS were dropped in that order onto the chip, which was left for one hour before being washed in absolute ethanol. Then, the same steps to immobilize streptavidin were implemented on the surface. The cellular specimen included ovary cancer cells and adenocarcinoma cells. One of each cell was stained with India ink (Becton and Dickinson Company, Mexico) to highlight the nuclei structure and assist comparisons between the DFM optical images.

C. Measurement System

An inverted microscopy (Axiovert200, Zeiss, Germany) equipped with a high sensitivity EMCCD (Luca, Andor, U.S.A.) was used to image the nanostructures and cellular specimen. Spectroscopic information was obtained by using a double-pass spectrograph (HR550, Jobin Yvon, U.S.A.) with a fiber optical bundle (200 μm) to collect the scattering light with Ti: Sapphire laser source (Tsunami®, Spectra-Physics, U.S.A.) under continuous mode. We have used a nonlinear optical crystal (TP 2000B, Photop Technologies, China) to generate 390 nm second harmonic light for UV illumination. Visible light region (400–700 nm) was obtained by passing the light from a halogen lamp (100W HAL lamp) through a built-in band pass filter. Fig. 1(a) depicts the schematic setup of the whole system and Fig. 1(b) depicts the alternative path of incident light in the transmitted and reflected modes. A 100X dark field objective lens ($NA = 0.75$, Zeiss, Germany) under reflective mode was utilized to image the one-dimensional nanostructures and to collect reflective spectra. For cellular structures of ovary cancer cells and adenocarcinoma cells, we have used transmitted mode to image the fixed samples on glass slide using a 100X lens. High numerical aperture (NA) of an oil-immersed condenser ($NA = 1.4$) and oil-immersed objective lens ($NA = 0.75$ to 1.3) were used in this system. All AFM images of optical disks were obtained in contact mode with AFM probe (PNP-DB) from Nanosensors™ (U.S.A.) with a spring constant of 0.06 N/m. The AFM images of the protein nanoarray were obtained in tapping mode with a spring constant of 48 N/m and a frequency of 190 kHz (Pacific Nanotechnology Instrument, U.S.A.).

D. Image and Signal Process

AFM images were analyzed with NanoRule++ (Pacific Nanotechnology Instrument, U.S.A.). DFM images were processed using NI Vision Assistant 8.0 (National Instruments, U.S.A.) to select the DFM images of the proper size for comparison with the AFM image. All spectra herein were the average of three acquired spectra and were all subtracted from the background spectrum from a white reflective object. The absorption spectrum of a thin gold layer with the same thickness on a smooth glass substrate was used as reference to calculate the shifts of SPR peaks.

III. Results and Discussion

Optical microscopic resolution is particularly important for the imaging of nanostructures and intracellular microstructures.

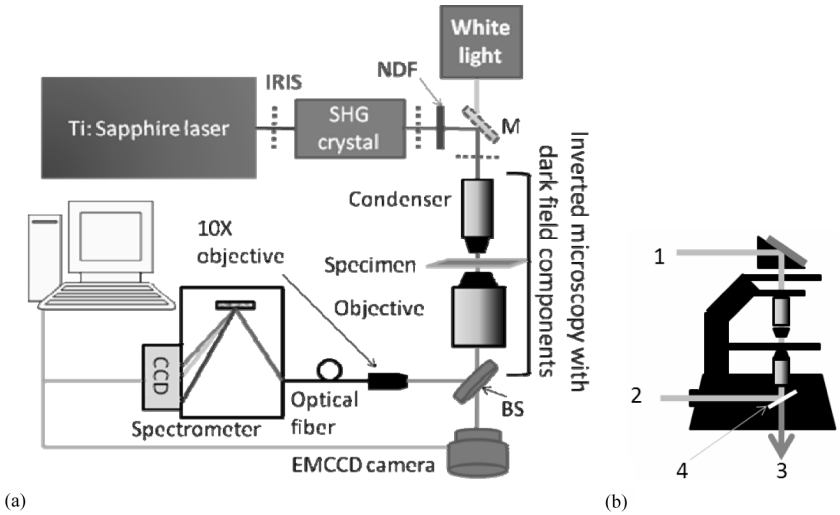

Fig. 1. (a) Schematic diagram of DFM with both imaging and spectral measurement functions, where *M* is reflected mirror, NDF is neutral density filter, and BS is beam splitter. Inverted microscopy (Axiovert200, Zeiss, Germany) and EMCCD (Luca, Andor, USA) were used to image nanostructures and cellular specimen under either reflective or transmitted modes. Spectroscopy (HR550, Jobin Yvon, USA) with a 10× objective lens to collect focused light through an optical fiber bundle to obtain the spectral information. A nonlinear optical crystal (TP 2000B, Photop Technologies, China) is used to generate 390 nm second harmonic light for UV illumination. Visible light region (400–700 nm) was obtained by passing the light through a built-in bandpass filter from a 100-W HAL lamp. (b) Diagram to represent the light path. Path 1 is light path of transmitted mode. Path 2 is light path of reflected mode. Path 3 is the light from specimen, and 4 is the reflector module within the microscopy.

In this study, commercially available optical disks were used to verify the performance of such systems. The track patterns of various optical disks are excellent calibration samples with consistent quality for the verification of system performance. In the first step, a white light source (400–700 nm) was used in the DFM system to acquire reflective images and compared with the corresponding AFM images. Fig. 2(a) shows a typical surface structure of an optical disk, which has "groove" for recording tracks and "land" for guiding tracks. The height and track pitch of such a surface structure vary with the different density formats. Fig. 2(b)–(e) shows images of track patterns taken from video compact disc (VCD) [Fig. 2(b)], 4.7 G digital video disc (DVD) [Fig. 2(c)], 8.5 G DVD [Fig. 2(d)], and 25 G Blu-ray disc [Fig. 2(e)], with corresponding AFM images on the left-hand side and reflective DFM images on the right-hand side. Consistent with the nominal specifications of these optical disks, both AFM and DFM methods revealed the same "land–groove" track pitches. The patterns of various optical disks can be clearly identified by DFM using white light. Furthermore, the last two images show a wobbly line pattern, commonly seen in optical disks. Pits of various sizes are also present on the bright lines, as can be seen in Fig. 2(c). Since the nominal pit width in the 25 G Blu-ray disc is 200 nm and the track pitch is 320 nm, the groove distance is calculated to be 120 nm. According to Fig. 2(e), in which white bands represent land and black bands are the grooves, the resolving power can reach and even exceed 120 nm, based on the current system setup. The size of the tract patterns was obtained from the full-width at half-maximum (FWHM) of the horizontal line profiles in DFM images. The nominal value was a linear function of the measured data: $y = 1.095x$ with an R^2 of 0.996, as shown in Fig. 2(f). The detection limit is about 129.6 nm, based on an assumed SNR of 3 with a calculated standard deviation of 47.3 nm (see Table I), or approximately 86.39 nm on the basis of an assumed SNR of 2. This value is close to the pixel size (86.6 nm) as determined under a 100× objective lens with dark-field components and a white light source.

To enhance the resolution, laser light with a wavelength of 390 nm was adopted to image the track patterns of a 25G Blu-ray disc [see Fig. 3(b)]; this image was then compared to the AFM image [see Fig. 3(c)]. The image produced thinner track lines than patterns imaged with white light [see Fig. 3(a)]. To measure the track sizes, the horizontal line profiles were obtained from DFM and AFM images, as shown in Fig. 3(d)–(f). From the FWHM of a horizontal line profile shown in Fig. 3(d) and (e), using white light and 390 nm UV light, the groove width is determined to be 245.37 ± 35.35 nm $(N = 6)$ and 151.55 ± 35.35 nm $(N = 6)$, respectively. assumed SNR of 2, the detection limit associated with the use of UV light is 70.7 nm $(151.55 \pm 35.35$ nm). On the basis an assumed SNR of 1, the lowest resolving width in this system is approximately 35.35 nm. The DFM image has not only high contrast, but abundant information concerning the scattering of light caused by the interaction of angular incident and orderly nanostructures. The resolution of DFM can thus be improved by collecting the scattered light through interference or surface plasmon enhancement. During the experiment, the resolution is also limited by the pixel size of the imaging system, and is improved by replacing a objective lens with high number aperture and replacing a charge-coupled device (CCD) camera with one with smaller pixels.

The FWHM of a horizontal line profile was then measured from these acquired images. Interestingly, all of the DFM values substantially exceed those obtained from the AFM, according to the paired *t*-test. However, the values determined from the AFM images are smaller than the nominal values, while the values from DFM are larger than expected. Although artifacts in the AFM images may be related to the probe characteristics, the magnification of the DFM images might be attributable to the refractive index of the substrate and the near-field evanescent effect. Another important limiting factor is the pixel

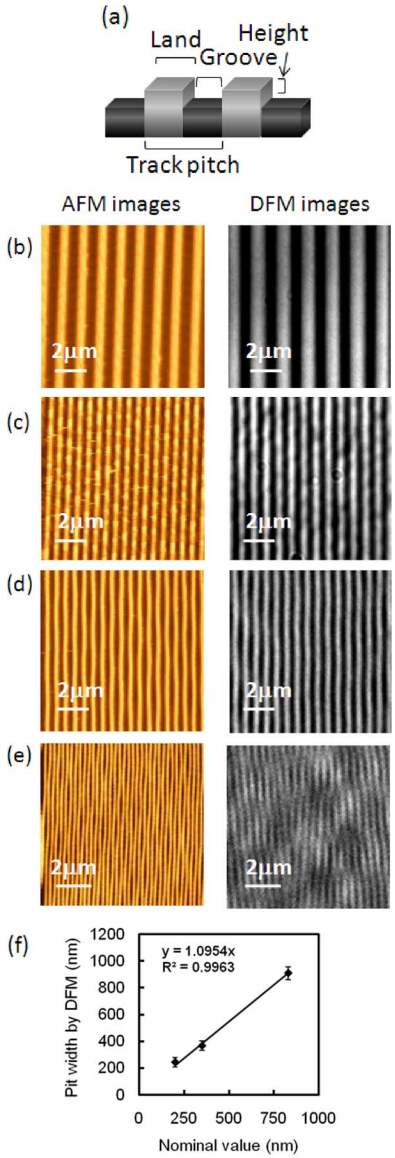

Fig. 2. (a) Diagram of general optical disk, and AFM and DFM images of: (b) VCD track; (c) 4.7 G DVD track; (d) 8.5G DVD track; and (e) 25G Blu-ray disc track. The bright band is the "land" and the black band is the "groove" in the typical "land–groove" structure of optical disks. Wobbly line patterns of high density optical disks are clearly observed in (d) and (e). (f) Relationship of nominal value versus pit width by DFM.

size of the CCD camera. Since the observations are made on a subwavelength scale, the effects of these factors in determining the quality of the image of the nanostructure are very important. Table I summarizes the measurements of the track patterns made from both DFM and AFM images. With the same nominal specifications, the measured track pitches and pit widths drop as the density of storage tracks increases. However, the standard deviations of the track widths from the DFM images are larger than the corresponding AFM values, possibly because the effective pixel size in the DFM system is larger. In the DFM system, the size of the pixels in the specification of the CCD camera is one factor that affects the resolution of the image. The pixel size corresponded to an image size of 86.6 nm in the presented system with a 100× objective lens, and the size of the AFM image is 19.53 nm per pixel over a scanning area of $10 \times 10\ \mu\text{m}^2$ a 512×512 matrix. 4.7G and 8.5G DVD are a single-sided single-layered disk and a single-sided double-layered disk, respectively. Therefore, the nominal track patterns in 4.7 G and 8.5 G DVD are the same, but the corresponding results herein differ slightly. The differences between the track patterns of 4.7 G and 8.7 G DVD in the DFM images are 93.81 nm, but that in the AFM images is 43.79 nm. For a Blu-ray disc, the nominal pitch is 320 nm and the groove width is 120 nm, based on the assumption that the land width equals the pit width. The width measured from the AFM image is 131.64 nm, but that in the DFM image with white light is 245.37 nm, and that in the DFM image with UV light is 151.55 nm. A value closer to the nominal value is obtained using monochromic light with a shorter wavelength, according to the diffraction equation $R = \lambda/2\text{NA}$, where R is the resolution and NA is the numerical aperture of the objective lens. Again, this effective magnification can be attributed to the near-field evanescent effect of the nanostructure [12], [18].

The nanostructure of the optical disks can act as a grating coupler in surface plasmon resonance (SPR) sensors [19]. However, recording dyes and protective coating layers somewhat affect its optical properties. To study their SPR behavior, absorption spectra of each sample were obtained with reference to a white reflective surface. Fig. 4 shows the absorption spectra with various 1-D track patterns. All absorption spectra are the differential results of reflective spectra from white surface and optical disks. Hence, the characteristics of all disk tracks depend strongly on the materials in the disk, such as the dye recording layer, the metallic reflector, and the substrate (polycarbonate). For example, the torn Blu-ray disc and VCD specimens in this experiment include a metallic reflector and a substrate, while the 4.7G DVD includes a dye recording layer and a metallic reflector. All spectra were normalized to their maximal value for qualitative comparison. A Gaussian function was then fitted to the absorption peaks to determine the central wavelength. Accordingly, the absorption peak plotted as circles of the VCD are located at a wavelength of 610 nm. The line plotted through the squares represents the absorption curve of the 4.7 G DVD, with an absorption band at 597 nm. The dashed line with absorption peak at 605 nm is measured from an 8.5 G DVD. The solid line is obtained from the Blu-ray disc, with a main peak at 590 nm.

To elucidate the plasmonic characteristics that are affected by various 1-D nanostructures, a 50-nm gold film was deposited on the surface of each disk sample. Fig. 5 shows the resultant absorption spectra of 1-D nanostructures with 50-nm gold film on top. The absorption peaks of each optical disk sample are at 600 nm (solid line, Blu-ray disc), 632 nm (dashed line, 8.5 G DVD), 593 nm (square line, 4.7 G DVD), and 600 nm (circle line, VCD), and 610 nm (smooth glass substrate as reference). The absorption peaks of these spectra from the disks with gold film differ from the measured reflective spectra of bare disks, as shown in Fig. 4. This difference suggests that absorption spectra of these disks are less influenced by the optical characteristics of the composed materials in different disks. Instead, the optical characteristics in these absorption spectra heavily depend on the pitches and groove depths of these disks.

Table II presents the identified absorption peak positions of spectral bands shown in Figs. 4 and 5, and clearly reveals the

TABLE I
SUMMARY AND COMPARISON OF NOMINAL FEATURE SIZES AND MEASURED DATA FROM BLU-RAY DISC, 8.5 G DVD, 4.7 G DVD, AND VCD BY DFM AND AFM

Specimen / Width by image type	Blu-ray Disc	8.5 G DVD	4.7 G DVD	VCD
Nominal pitch width (nm)*	320	740		1600
Nominal pit width (nm)*	200	350		830
Pit width (nm)+ by DFM	**245.37**±35.35 (**151.55**±35.35)**	**368.05**±36.23	**461.87**±44.72	**909.3**±47.43
Pit width (nm)# by AFM	**131.64**±19.07	**262.50**±19.44	**306.29**±29.90	**549.67**±23.67
Depth (nm) by AFM	**17.62**±0.49	**87.28**±1.56	**83.17**±3.31	**116.70**±4.03

Note: (*) width values are the general standards for optical disks. (+) width values of pit are determined from DFM images and (**) width values is obtained from UV images. (#) width values of pit are calculated from the FWHM of the line profile in AFM images.

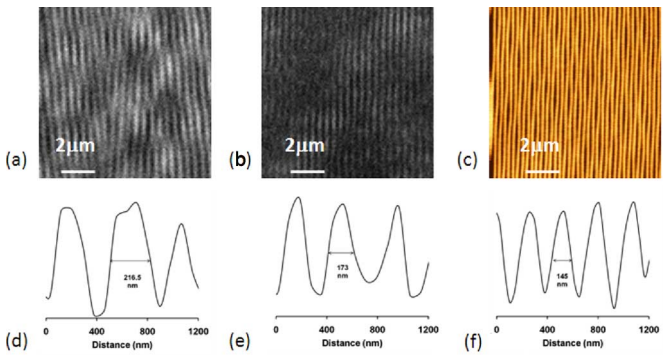

Fig. 3. Comparisons of resolution of DFM from images from a 25 G Blu-ray disc using different light sources: (a) white light, (b) 390 nm UV laser; and (c) corresponding AFM image. (d)–(f) Corresponding line profiles of (a)–(c).

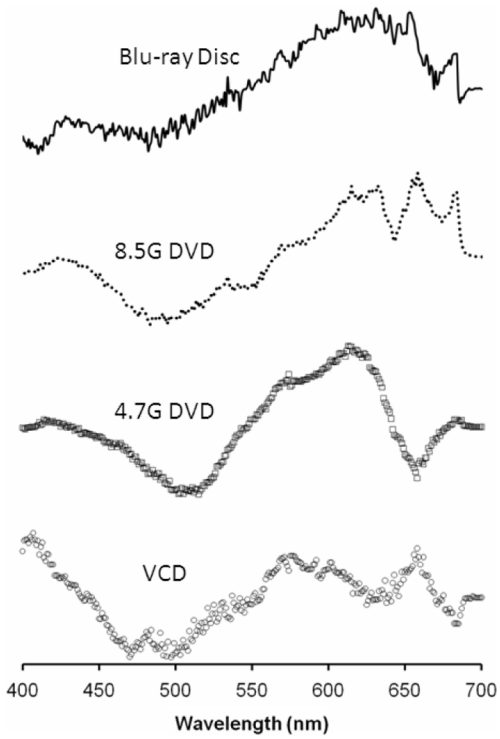

Fig. 4. Absorption spectra of various optical disks after subtraction of reflection spectrum of a white surface. Solid line is absorption spectrum of Blu-ray disc; dashed line is that of 8.5 G DVD; line through squares is that of 4.7 G DVD; and line through circles is that of VCD. The curves have been offset for clarity.

shift in the absorption band caused by the thin gold layer. As presented in Table II, the plasmonic effect of the thin gold layer at various nanostructure widths shifts the absorption bands from 593 to 632 nm. On the basis of the surface plasmonic properties of a grating coated with a noble metal, increasing the grating width causes redshifts of the absorption band, and increasing the grating height causes blueshifts of the absorption band [20]. The results shown in Fig. 5 indicate a redshift of the spectral peaks of the Blu-ray disc and the 8.5 G DVD, while those of the 4.7 G DVD and VCD are blueshifted. Comparing the groove depths in the AFM images (see Table I) reveals that the height of the VCD track is six times that of the Blu-ray disc, thus causing a blueshift. Singh *et al.* obtained the transmission spectra of the gold-coated DVD-R and found that the absorption peaks are at around 500 and 640 nm [21]. Their specimen did not include a metal reflector. The 8.5 G DVD specimen in this paper also contains a dye recording layer and substrate, so the absorption band at 632 nm was similar to that identified by Singh *et al.* Conversely, the absorption band at 593 nm in 4.7 G DVD is blueshifted because the specimen includes a metal reflector that affects the resonance of the surface plasmon.

To evaluate the optical performance of a biological specimen, biomolecules and cultured cells were prepared for both imaging and spectral analyses. Surface plasmon enhancement due to thin metallic film provides a highly sensitive mechanism for detecting biomolecules on the surface. A Blu-ray disc was prepared with an Au coating and labeled with biomolecules, streptavidin. Fig. 6 shows the absorption spectra of labeled and nonlabeled surfaces. The plasmonic peak shifted from 600 to 610 nm when a Gaussian function was used to find the optimal central position of absorption peak in a nonlinear curve fitting process, revealing that this system can be applied to sense biomolecular interactions based on SPR enhancement. The estimated results indicate that the resolution of DFM in this paper is about 86 nm. A silicon dioxide nanoarray that measures 70 μm $\times$ 70 μm with spot size of 50 nm was then fabricated by using an electrically biased AFM tip on a silicon wafer. Streptavidin was then selectively immobilized on these nanodots using a previously mentioned procedure. Fig. 7(a)

TABLE II
COMPARISON OF ABSORPTION PEAKS OF VARIOUS OPTICAL DISKS AND DISK COATED WITH GOLD LAYER

Specimen	Blu-ray Disc (160 nm)	8.5G DVD (320 nm)	4.7G DVD (360 nm)	VCD (600 nm)
Bare disk surface	590 nm	605 nm	597 nm	610 nm
Disk surface with 50 nm gold film	600 nm	632 nm	593 nm	600 nm

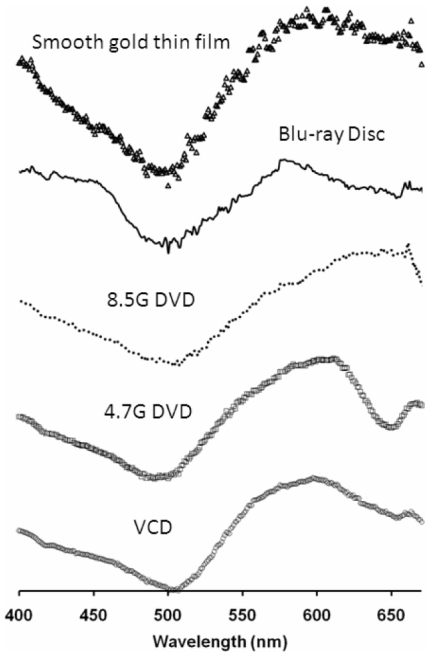

Fig. 5. Curve plotted through triangles is the absorption spectrum of a 50-nm-thick smooth gold film deposited on a glass substrate. The reflection spectrum of a white surface has been subtracted from the curves. Absorption spectra of various optical disks coated with a 50-nm-thick gold film are plotted overlayingly for comparison, which are Blu-ray disc (solid line), 8.5 G DVD (dashed line), 4.7 G DVD (squares line), and VCD (circles line).

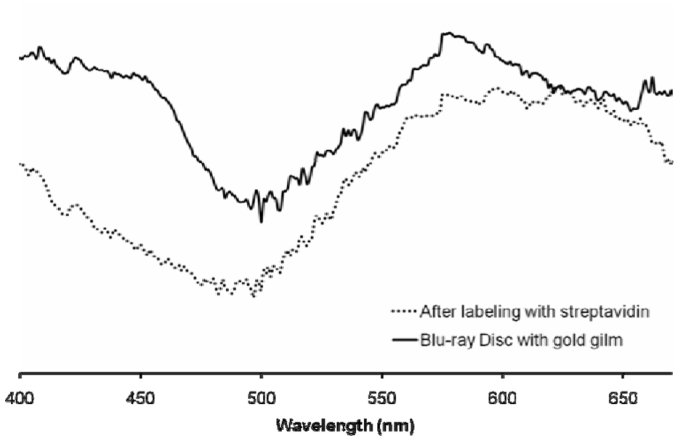

Fig. 6. Absorption spectra of Blu-ray disc coated with 50-nm-thick gold film (solid line) and with surface that is adhered immobilized streptavidin (dashed line).

shows a 3-D AFM image of the resultant nanoarray. The measured molecular heights are 4.21 ± 0.55 nm, which is close to the theoretical value for streptavidin [22]. Under reflective mode of DFM with white light, we can easily identify the appearance of fabricated nanoarray [see Fig. 7(b) and (c)].

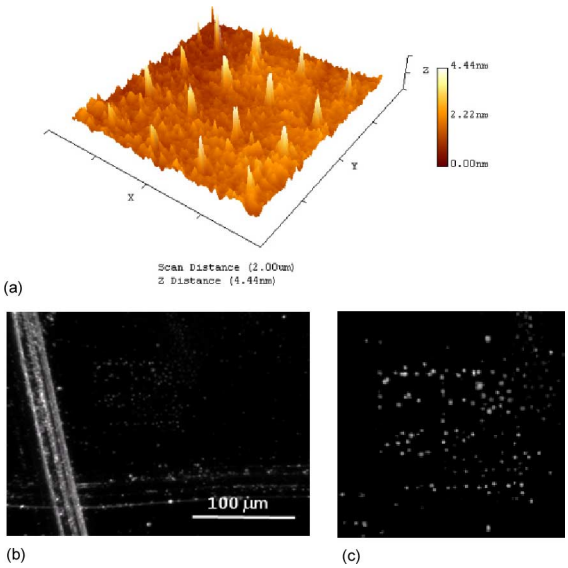

Fig. 7. (a) 3-D AFM image with scan area of 2 μm×2 μm. The scales on the x and y axes run to 500 nm. (b) DFM image of nanoarray. (c) Magnification of the square area in (b) of the nanoarray image.

This DFM system was then used to image cultured cells for the preliminary determination of cellular structures. Coating 1-D nanostructures with a thin layer of noble metal can yield local information about possible molecular interactions. In this paper, two species of cultured cells, adenocarcinoma and ovary cancer, were imaged under the transmitted light for both bright-field microscopy and DFM with an oil immersion objective lens. The nuclei of adenocarcinoma cells were stained before imaging. Fig. 8(a) depicts the dense nuclei structures with a sharp contrast at the boundary between the cytoplasm and the nuclei. Details of the internal components are identified in both bright-field and dark-field images. Nuclei enlarged to about 18 μm are a distinctive feature of the cancer cells. Unstained ovary cancer cells are also adopted as specimens to be similarly examined to obtain bright-field and dark-field images. Fig. 8(b) demonstrates that cells are highly transparent in the bright-field image and barely distinguishable at the membrane boundary. In contrast, the cellular boundaries can be clearly identified in the dark-field image, because of the high sensitivity of DFM to edges in the specimen. This finding indicates not only the potential of using DFM to image living cells without staining, but also the possibility of enhancing the signals associated with intracellular interactions of biomolecules.

Although the resolution of DFM is not as efficient as that of AFM, DFM combined with spectral information has many advantages over AFM in highly detailed near-surface characterization. First, although the DFM system can obtain an image and optical spectra of a specimen to analyze its optical properties,

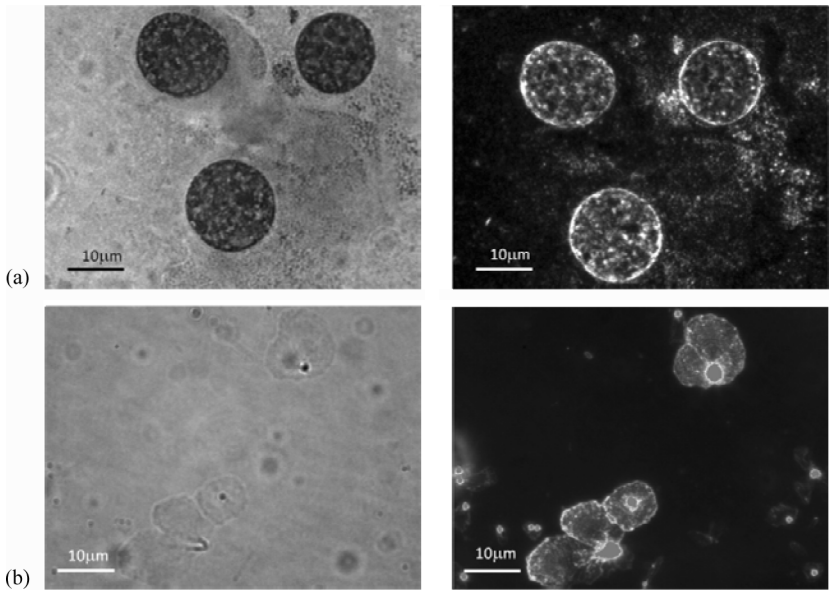

Fig. 8. (a) (Left-hand side) Bright-field image and (right-hand side) dark-field image of stained Adenocarcinoma for identification of nuclei structures and (b) (left-hand side) bright-field image and (right-hand side) dark-field image of unstained ovary cancer cells.

the AFM image provides only information on the size of the specimen. Second, although the DFM system can monitor continuously all biomolecular interactions without any mechanical disturbance, AFM can only verify morphological changes in the steady state. Third, although the area of observation in the most AFM systems is limited to 100 μm$\times$100 μm, the objective lens in DFM can be changed for practical applications. The result shown in Fig. 7 also indicates the potential of using a protein nanoarray on optical disks in the future.

IV. Conclusion

This paper presents a combined DFM and spectral measurement system to observe intracellular structures, and classifies the biomolecular interactions of a nanostructure coated with a noble metal. To test the resolution of this optical image system, nanofeatures with widths of 120–770 nm were imaged by DFM, and the sizes of the patterns were confirmed by AFM imaging. The results show that the current resolution of DFM is approximately 86 nm, and that the DFM image is larger than the AFM image. For nanofeatures with various pitch sizes, a 50-nm gold layer was deposited using an e-beam evaporator; this layer served as SPR-active substrate. The absorption spectra were obtained to identify the surface plasmon properties induced by the thin gold film. Specimens of adenocarcinoma cells and ovary cancer cells were also imaged using DFM, and the structures of the nuclei and some cellular organs were clearly identified using a 100 $\times$objective lens and electron-multiplying CCD (EMCCD). On the basis of the current results, this optical system has the capacity to generate images of biomolecular interactions that occur inside a cell.

Acknowledgment

The cellular specimens were prepared by M. S. Su-Yu Chu, who is the Director of the Division of Clinical Microscopy, National Taiwan University Hospital, Taiwan. T. Knoy is appreciated for his editorial assistance.

References

[1] A. Campion and P. Kambhampati, "Surface-enhanced Raman scattering," *Chem. Soc. Rev.*, vol. 27, pp. 241–250, 1998.

[2] K. Kneipp, H. Kneipp, I. Itzkan, R. R. Dasari, and M. S. Feld, "Surface-enhanced Raman scattering and biophysics," *J. Phys., Condens. Matter*, vol. 14, pp. R597–R624, 2002.

[3] H. Xu and M. Kall, "Modeling the optical response of nanoparticle-based surface plasmon resonance sensors," *Sens. Actuators B, Chem.*, vol. 87, pp. 244–249, 2002.

[4] K. Brunner, G. Abstreiter, G. Böhm, G. Tränkle, and G. Weimann, "Sharp-line photoluminescence and two-photon absorption of zero-dimensional biexcitons in a GaAs/AlGaAs structure," *Phys. Rev. Lett.*, vol. 73, pp. 1138–, 1994.

[5] K. Tai, A. Mysyrowicz, R. J. Fischer, R. E. Slusher, and A. Y. Cho, "Two-photon absorption spectroscopy in GaAs quantum wells," *Phys. Rev. Lett.*, vol. 62, pp. 1784–, 1989.

[6] K. Choi, H. Kim, Y. Lim, S. Kim, and B. Lee, "Analytic design and visualization of multiple surface plasmon resonance excitation using angular spectrum decomposition for a Gaussian input beam," *Opt. Exp.*, vol. 13, pp. 8866–8874, 2005.

[7] R. Naraoka and K. Kajikawa, "Phase detection of surface plasmon resonance using rotating analyzer method," *Sens. Actuators B, Chem.*, vol. 107, pp. 952–956, 2005.

[8] J. Homola, "On the sensitivity of surface plasmon resonance sensors with spectral interrogation," *Sens. Actuators B, Chem.*, vol. 41, pp. 207–211, 1997.

[9] C.-W. Lin, K.-P. Chen, C.-N. Hsiao, S. Lin, and C.-K. Lee, "Design and fabrication of an alternating dielectric multi-layer device for surface plasmon resonance sensor," *Sens. Actuators B, Chem.*, vol. 113, pp. 169–176, 2006.

[10] C.-W. Lin, K.-P. Chen, M.-C. Su, T.-C. Hsiao, S.-S. Lee, S. Lin, X.-J. Shi, and C.-K. Lee, "Admittance loci design method for multilayer surface plasmon resonance devices," *Sens. Actuators B, Chem.*, vol. 117, pp. 219–229, 2006.

[11] N. Fang, H. Lee, C. Sun, and X. Zhang, "Sub-diffraction-limited optical imaging with a silver superlens," *Science*, vol. 308, pp. 534–537, Apr. 2005.

[12] I. I. Smolyaninov, Y.-J. Hung, and C. C. Davis, "Magnifying superlens in the visible frequency range," *Science*, vol. 315, pp. 1699–1701, Mar. 2007.

[13] K. I. Willig, S. O. Rizzoli, V. Westphal, R. Jahn, and S. W. Hell, "STED microscopy reveals that synaptotagmin remains clustered after synaptic vesicle exocytosis," *Nature*, vol. 440, pp. 935–939, 2006.

[14] E. Auksorius, B. R. Boruah, C. Dunsby, P. M. P. Lanigan, G. Kennedy, M. A. A. Neil, and P. M. W. French, "Stimulated emission depletion microscopy with a supercontinuum source and fluorescence lifetime imaging," *Opt. Lett.*, vol. 33, pp. 113–115, 2008.

[15] A. D. McFarland and R. P. VanDuyne, "Single silver nanoparticles as real-time optical sensors with zeptomole sensitivity," *Nano Lett.*, vol. 3, pp. 1057–1062, 2003.
[16] B. Dragnea, C. Chen, E. S. Kwak, B. Stein, and C. C. Kao, "Gold nanoparticles as spectroscopic enhancers for in vitro studies on single viruses," *J. Amer. Chem. Soc.*, vol. 125, pp. 6374–6375, 2003.
[17] R. Danczyk, B. Krieder, A. North, T. Webster, H. HogenEsch, and A. Rundell, "Comparison of antibody functionality using different immobilization methods," *Biotechnol. Bioeng.*, vol. 84, pp. 215–223, 2003.
[18] N. Fang, Z. Liu, T. J. Yen, and X. Zhang, "Experimental study of transmission enhancement of evanescent waves through silver films assisted by surface plasmon excitation," *Appl. Phys. A, Mater. Sci. Process.*, vol. 80, pp. 1315–1325, 2005.
[19] N.-F. Chiu, C.-W. Lin, J.-H. Lee, C.-H. Kuan, K.-C. Wu, and C.-K. Lee, "Enhanced luminescence of organic/metal nanostructure for grating coupler active long-range surface plasmonic device," *Appl. Phys. Lett.*, vol. 91, pp. 083114-1–083114-3, 2007.
[20] L. Gaetan and J. F. M. Olivier, *Numerical Study and Optimization of a Diffraction Grating for Surface Plasmon Excitation*, I. S. Mark, Ed. Bellingham, WA: SPIE, 2005, vol. 5927, pp. 592713-1–592713-9.
[21] B. K. Singh and A. C. Hillier, "Surface plasmon resonance enhanced transmission of light through gold-coated diffraction gratings," *Anal. Chem.*, vol. 80, pp. 3803–3810, 2008.
[22] C. A. Helm, W. Knoll, and J. N. Israelachvili, "Measurement of ligand-receptor interactions," *Proc. Nat. Acad. Sci. USA*, vol. 88, pp. 8169–8173, Sep. 1991.

Hui-Hsin Lu received the M.S. degree from the Institute of Biomedical Engineering, National Yang-Ming University, Taipei, Taiwan, in 2004, and the Ph.D. degree in electrical engineering from the National Taiwan University, Taipei, in 2009.

From October 2004 and April 2005, she was an Assistant Engineer at the Institute of Nuclear Energy Research, Taiwan, where she responded for simulation of dosimetric distribution of waste from nuclear power plant. She is currently a Postdoctoral Fellow in the Institute of Biomedical Engineering, National Taiwan University. Her research interests include nanophotonics and bionano-electromechanical systems.

Tzu-Chien Hsiao received the M.S. degree from the Institute of Physics, National Sun Yat-Sen University, Kaohsiung, Taiwan, in1994, and the Ph.D. degree from the Institute of Biomedical Engineering, National Yang-Ming University, Taipei, Taiwan, in 2003.

From 2003 to 2006, he was an Assistant Professor at the Institute Biomedical Engineering, I-Shou University, Kaohsiung. From 2004 to 2006, he was also the Deputy Director of the Biomedical Research and Development Division, Hsinchu Biomedical Science Park. Since 2006, he has been an Assistant Professor in the Department of Computer Science and the Institute of Biomedical Engineering, National Chiao Tung University, Hsinchu, Taiwan. His research interests include neural networks, virtual instrument, and multivariate spectral analysis.

Su-Ming Hsu received the M.D. degree from the College of Medicine, National Taiwan University, Taipei, Taiwan, in 1974.

He was with the Department of Pathology and Laboratory Medicine, University of Texas Health Science Center, Houston. He was the Director of hematopathology and immunopathology, Department of Pathology, University of Arkansas for Medical Science, from 1977 to 1995. From 1997 to 2004, he was the Vice-Superintendent for Research at the College of Medicine, National Taiwan University, where he is currently a Professor in the Department of Pathology. He was the Chief Executive Officer of Hsin-Chu Biomedical Science Park Project from 2003 to 2006. He has been awarded many honors and other scientific recognitions since 1976. The significance of his research is reflected by the fact that his research papers have been cited more than 15 000 times up to now.

Chii-Wann Lin (M'95) received the B.S. degree from the Department of Electrical Engineering, National Cheng-Kung University, Tainan, Taiwan, in 1984, the M.S. degree in biomedical engineering from the Graduate Institute of Biomedical Engineering, National Yang-Ming University, Taipei, Taiwan, in 1986, and the Ph.D. degree in biomedical engineering from the Case Western Reserve University (CWRU), Cleveland, OH, in 1993.

From January 1993 to August 1993, he was a Research Associate in the Neurology Department, CWRU. From September 1993 to August 1998, he was with the Center for Biomedical Engineering, College of Medicine, National Taiwan University. He is currently a Professor in the Graduate Institute of Biomedical Engineering, National Yang-Ming University. He also holds a joint appointments in the Department of Electrical Engineering and the Institute of Applied Mechanics, National Taiwan University, Taipei, Taiwan. His research interests include biomedical micro sensors, optical biochip, surface plasmon resonance, bioplasmonics, nanomedicine, and personal e-health system.

Prof. Lin is also a member of the IEEE Engineering in Medicine and Biology Society, the International Federation for Medical and Biological Engineering, and the Chinese Biomedical Engineering Society. He is the President of Taiwan Association of Chemical Sensors from 2008 to 2010.